

Weinberg eigenvalues for chiral nucleon-nucleon interactions

J. Hoppe,^{1,2,*} C. Drischler,^{1,2,†} R. J. Furnstahl,^{3,‡} K. Hebeler,^{1,2,§} and A. Schwenk^{1,2,4,¶}

¹*Institut für Kernphysik, Technische Universität Darmstadt, 64289 Darmstadt, Germany*

²*ExtreMe Matter Institute EMMI, GSI Helmholtzzentrum für Schwerionenforschung GmbH, 64291 Darmstadt, Germany*

³*Department of Physics, The Ohio State University, Columbus, OH 43210, USA*

⁴*Max-Planck-Institut für Kernphysik, Saupfercheckweg 1, 69117 Heidelberg, Germany*

We perform a comprehensive Weinberg eigenvalue analysis of a representative set of modern nucleon-nucleon interactions derived within chiral effective field theory. Our set contains local, semilocal, and nonlocal potentials, developed by Gezerlis, Tews *et al.* (2013); Epelbaum, Krebs, and Meißner (2015); and Entem, Machleidt, and Nosyk (2017) as well as Carlsson, Ekström *et al.* (2016), respectively. The attractive eigenvalues show a very similar behavior for all investigated interactions, whereas the magnitudes of the repulsive eigenvalues sensitively depend on the details of the regularization scheme of the short- and long-range parts of the interactions. We demonstrate that a direct comparison of numerical cutoff values of different interactions is in general misleading due to the different analytic form of regulators; for example, a cutoff value of $R = 0.8$ fm for the semilocal interactions corresponds to about $R = 1.2$ fm for the local interactions. Our detailed comparison of Weinberg eigenvalues provides various insights into idiosyncrasies of chiral potentials for different orders and partial waves. This shows that Weinberg eigenvalues could be used as a helpful monitoring scheme when constructing new interactions.

I. INTRODUCTION

Chiral effective field theory (EFT) has become the standard method to generate microscopic nuclear Hamiltonians for few- and many-body calculations. The dominant implementation is based on nucleon and pion degrees of freedom (i.e., without explicit delta resonances) and an organization dictated by the EFT power counting known as Weinberg counting. This specifies a diagrammatic expansion for inter-nucleon potentials, which has been described in detail in several reviews (e.g., see Refs. [1, 2]). But while the diagrammatic content is prescribed, a potential requires specifying an ultraviolet regularization scheme with an associated scale parameter or possibly different parameters in separate many-body sectors. Such a scheme includes additional freedom in choosing the functional form of the regulator function. Thus, there is an infinite variety of candidate potentials to describe low-energy nuclear phenomena.

Up to a few years ago, a particular chiral EFT nucleon-nucleon (NN) potential, specified over a decade ago in Ref. [3] and supplemented with the leading three-nucleon (3N) interaction, was used in almost all many-body calculations (however, with different choices for 3N regulators and fits). Improvements in many-body methods and the advance of high-performance computing has enabled application to a wide variety of nuclear systems (e.g., see Refs. [4–7]). While there have been notable phenomenological successes, the improved precision and reach of these calculations have manifested deficiencies in the

Hamiltonian. As a result, various groups have revisited the construction and fitting of chiral potentials to better realize the EFT advantages of systematic order-by-order improvement with quantifiable errors.

Several different families (schemes) of nuclear interactions using Weinberg counting have been introduced, with a variety of parameter estimation methods used to fit the low-energy constants to nuclear data. These can be classified according to the regulator implementation (see Sec. II) as local, semilocal, or nonlocal, with broad freedom to choose the functional form of the regulator within each category. The NN interaction has been pushed to fifth order in Weinberg counting (“next-to-next-to-next-to-next-to-leading order” or N^4 LO) [8–10], although for consistency with 3N interactions various other lower order NN interactions are available and have been applied. In principle, these interactions should all be capable of describing the same phenomena, but in practice the detailed differences can be important. While effects of the regulator (so-called regulator artifacts) at a given order in the expansion are supposed to be removed systematically at higher orders, actual calculations show significant influence of artifacts on the EFT convergence pattern. In this work, we apply the eigenvalue analysis methods developed by Weinberg [11] (see also Refs. [12–14]) to compare several sets of chiral NN potentials.

The Weinberg eigenvalue analysis is a versatile diagnostic tool to quantify the perturbativeness of nuclear interactions and provide insight into the physics of individual partial-wave channels. Originally, Weinberg developed this method in the early 1960s while working to understand bound states in nonrelativistic quantum mechanics (as a warm-up to understanding composite particles in quantum field theory) and how to introduce quasiparticles to cure nonconvergent Born series [11, 15]. More recent applications of the Weinberg analysis [16–21] provide quantitative insights into how renormalization-group

* Email: jhoppe@theorie.ikp.physik.tu-darmstadt.de

† Email: christian.drischler@physik.tu-darmstadt.de

‡ Email: furnstahl.1@osu.edu

§ Email: kai.hebeler@physik.tu-darmstadt.de

¶ Email: schwenk@physik.tu-darmstadt.de

TABLE I. Short- and long-range regulators for the local, semilocal, and nonlocal potentials of Refs. [9, 10, 22–25] with $\tilde{r} \equiv r/R_0$ and $\tilde{p} \equiv p/\Lambda$ in the second and third columns, where $\alpha = (\pi\Gamma(3/4)R_0^3)^{-1}$ is a normalization constant and ν is the order in the chiral expansion. For the EMN potentials, the regulator exponent $n_2 = 2$ is applied to the pion exchanges and $n_2 = 4$ for one-pion exchange beyond next-to-leading order (NLO). The highest available chiral order and the cutoff ranges are given in the fifth column, while the determination of the πN low-energy constants (LECs)/ 2π regularization and the fitting protocol are given in the second-to-last and the last columns, respectively. SFR and DR denote spectral-function and dimensional regularization, whereas PWA stands for partial-wave analysis.

	Regulator functions		Regulator	Chiral order/	$\pi N/$	Fitting protocol
	Short (contact)	Long (pion exchanges)	exponent(s)	cutoff range	2π regularization	
Local						
GT+ [22, 23]	$\alpha e^{-\tilde{r}^n}$	$1 - e^{-\tilde{r}^n}$	$n = 4$	Up to N ² LO $R_0 = 0.9 - 1.2$ fm	Fixed values from Ref. [26] SFR	Nijmegen PWA [27]
Semilocal						
EKM [9, 24]	$e^{-\tilde{p}^{n_1}} e^{-\tilde{p}'^{n_1}}$	$(1 - e^{-\tilde{r}^2})^{n_2}$	$n_1 = 2$ $n_2 = 6$	Up to N ⁴ LO $R_0 = 0.8 - 1.2$ fm $\Lambda \approx 493 - 329$ MeV	Fixed values [24] DR	Nijmegen PWA [27]
Nonlocal						
sim [25]	$e^{-\tilde{p}^{2n}} e^{-\tilde{p}'^{2n}}$	$e^{-\tilde{p}^{2n}} e^{-\tilde{p}'^{2n}}$	$n = 3$	Up to N ² LO $\Lambda = 450 - 600$ MeV	Fitting parameter in simultaneous fit SFR	Fits to NN , πN , and few-body systems $^2,^3\text{H}$, ^3He
EMN [10]	$e^{-\tilde{p}^{2n_1}} e^{-\tilde{p}'^{2n_1}}$	$e^{-\tilde{p}^{2n_2}} e^{-\tilde{p}'^{2n_2}}$	$n_1 > \nu/2$ $n_2 = 2$ (4)	Up to N ⁴ LO $\Lambda = 450 - 550$ MeV	Fixed values from Ref. [28] SFR	NN data from 1955-2016 [29]

(RG) techniques act in softening different components of nuclear interactions and how the effects of potentials are modified at finite density.

By perturbativeness we mean the order-by-order convergence pattern in a perturbative many-body expansion (which needs to be distinguished from an order-by-order convergence in the chiral EFT expansion). For NN scattering in free space, this expansion is the Born series. For many-body systems such as infinite matter and finite nuclei, this expansion is many-body perturbation theory (MBPT). While we are particularly interested in whether MBPT converges and at a practical rate (e.g., at low-enough order to be tractable), the characterization of perturbativeness is of more general concern. For nonperturbative many-body methods using a basis expansion, the computational resources for convergence depend strongly on perturbativeness. It is also relevant for identifying or justifying reference states such as Hartree-Fock and for motivating microscopic nuclear density functional theory.

The plan of the paper is as follows. In Sec. II we characterize three classes of regularization schemes used in recently formulated chiral NN interactions and critically compare regulator parameters. In Sec. III we review the relevant features of the Weinberg eigenvalue analysis, illustrating their general behavior in the complex plane,

and document the use of the eigenvalues to approximate phase shifts for modern interactions. Eigenvalues at different orders and in different partial-wave channels are given for the various chiral NN potentials in Sec. IV, highlighting differences from regulators and features at different orders, which also depend on the different types of regularization schemes. Section V contains our summary and outlook.

II. NN INTERACTIONS AND REGULARIZATION

During recent years there has been significant progress in developing new nuclear forces within chiral EFT (see, e.g., Refs. [9, 10, 22–25] including also explicit delta resonances in Refs. [30–32]). The development of novel advanced fitting frameworks, the exploration of new regularization schemes, and the derivation of more systematic ways to estimate theoretical uncertainties has resulted in new families of interactions that allow nuclei and nuclear matter to be systematically studied within *ab initio* frameworks at different orders in the chiral expansion.

In this section, we briefly summarize properties of these new interactions to prepare for diagnosing them using the Weinberg eigenvalue analysis. In particular, we focus on

three sets of potentials, commonly referred to as local, non-local, and semilocal, which are characterized by different regularization schemes to separate the long-distance from the short-distance physics. To be specific, we consider the local potentials of Refs. [22, 23] by Gezerlis, Tews, *et al.* (GT+), the semilocal potentials of Refs. [9, 24] by Epelbaum, Krebs, and Meißner (EKM), the nonlocal potentials of Ref. [25] by Carlsson, Ekström *et al.* (sim), and the nonlocal potentials of Ref. [10] by Entem, Machleidt, and Nosyk (EMN). Table I summarizes properties of these potentials including the specific form of the employed regulators as well as the available orders in the chiral expansion, the pion-nucleon (πN) low-energy constants (LECs), the 2π regularization, and the fitting protocols. For more detailed information, we refer to the given references.

Local interactions use regulators that only depend on the momentum transfer $\mathbf{q} = \mathbf{p}' - \mathbf{p}$ in momentum space or on the relative distance \mathbf{r} in coordinate space, respectively. Here \mathbf{p} and \mathbf{p}' denote the relative momenta of the initial and final two-body states. The derivation of local interactions in Refs. [22, 23] opened new ways for applying nuclear interaction from chiral EFT in quantum Monte Carlo (QMC) calculations [33–36]. The benefits of locally regularizing long-range physics such as the pion-exchange interactions are discussed in Ref. [24]. These include the conservation of the analytical structure of the T -matrix close to the pion threshold and the fact that no spectral function regularization (SFR) is needed in this regularization approach (see also Ref. [23]), with dimensional regularization (DR) applied in Ref. [24]. However, for the short-range couplings the local regularization leads to a mixing of different partial-wave channels due to the dependence of \mathbf{q} on the angle $\cos\theta_{\mathbf{p}\mathbf{p}'}$. As a consequence, S -wave short-range contact interactions generally induce nonvanishing contributions in higher partial waves after regularization [23], whereas for nonlocal regulators, which only depend on the magnitude of the relative momenta p and p' , such short-range interactions remain restricted to only S waves. This leads in particular to technical simplifications since different partial-wave channels can be fitted independently.

The semilocal EKM interactions [9, 24] combine the conceptual advantages of locally regularized long-range interactions with technical benefits of nonlocal short-range interactions. In practice, the regularization of the long-range parts is formulated in coordinate space and is characterized by a cutoff scale R_0 , whereas the short-range regularization is performed in momentum space which involves a cutoff scale Λ . Physically, it is a natural assumption that these two scales should be related. In Ref. [24], a mapping between the two scales was motivated by considering the Fourier transforms of Gaussians, which leads to the relation

$$\Lambda(R_0) = \frac{2}{R_0}. \quad (1)$$

In Ref. [23], a cutoff mapping between momentum and coordinate space was suggested by relating the integral over

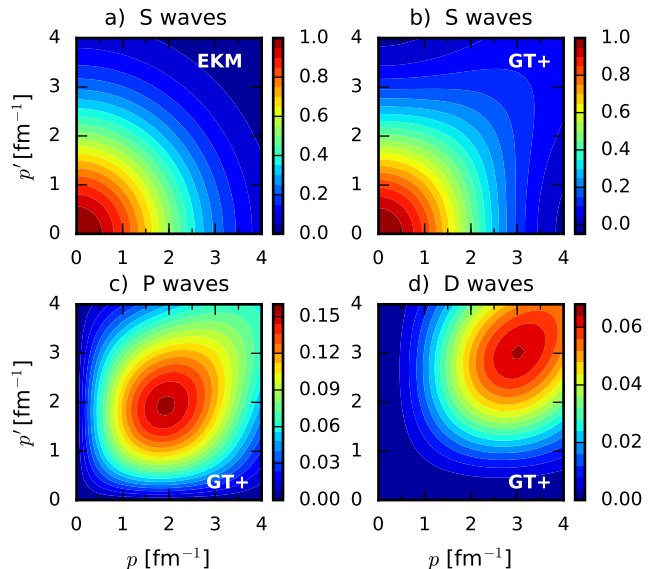


FIG. 1. (Color online) Contour plot for the short-range regulator of the GT+ and EKM potentials. (a) The nonlocal EKM regulator, which is independent of the angular momentum, is plotted for $\Lambda = 493$ MeV, while the local regulator, which depends on the partial wave, is shown in the (b) S , (c) P , and (d) D waves for the cutoff $R_0 = 1.2$ fm. We find good agreement in the S waves for the cutoff combination $R_0^{\text{GT}+} = 1.2$ fm and $R_0^{\text{EKM}} = 0.8$ fm, assuming Eq. (1). A least-squares minimization shows that the regulators in the S waves are most comparable for $R_0^{\text{EKM}} = 0.85$ fm.

the Fourier-transformed short-range regulator function (see Table I),

$$f_{\text{local}}(q^2, R_0) = \int d\mathbf{r} \alpha e^{-(r/R_0)^4} e^{-i\mathbf{q}\cdot\mathbf{r}}, \quad (2)$$

with the integral over a sharp momentum cutoff:

$$\int d\mathbf{q} f_{\text{local}}(q^2, R_0) = \int d\mathbf{q} \theta(\Lambda - |\mathbf{q}|). \quad (3)$$

Obviously, there is no universal way to relate the coordinate and momentum space cutoff scales. By comparing the numerical values for Λ resulting from relations (1) and (3) we obtain quite different numbers: for $R_0 = 0.8$ fm we get $\Lambda = 493$ and 614 MeV, whereas for $R_0 = 1.2$ fm, $\Lambda = 329$ and 409 MeV, respectively. In Fig. 1 we show a contour plot of the semilocal short-range regulator with $R_0^{\text{EKM}} = 0.8$ fm, i.e., $\Lambda = 493$ MeV in the S waves, and the Fourier transform of the local short-range regulator with $R_0^{\text{GT}+} = 1.2$ fm in the S , P , and D waves. We find good agreement in the S waves for this chosen cutoff combination, with a least-squares minimization indicating best agreement for $R_0 = 0.85$ fm for the semilocal potential. However, we observe in general a quite different behavior for the nonlocal versus the angular-dependent local regulator in momentum space, where the latter does not cut off contributions with $\mathbf{p} = \mathbf{p}'$. Furthermore, the q^2 -dependent contacts at NLO and beyond with $p \neq p'$ are

TABLE II. Distance r^* where the long-range regulator function takes the value $f_{\text{long}}(r^*, R_0) = 1/2$ for the GT+ (middle column) and EKM (right column) regulator functions; see Table I. Results are shown for a cutoff range of $R_0 = 0.8$ – 1.2 fm. We find best agreement for the cutoff combination $R_0^{\text{GT}+} = 1.2$ fm and $R_0^{\text{EKM}} = 0.8$ fm.

R_0 [fm]	$r_{\text{GT}+}^*$ [fm]	r_{EKM}^* [fm]
0.8	0.73	1.19
0.9	0.82	1.34
1.0	0.91	1.49
1.1	1.00	1.64
1.2	1.10	1.79

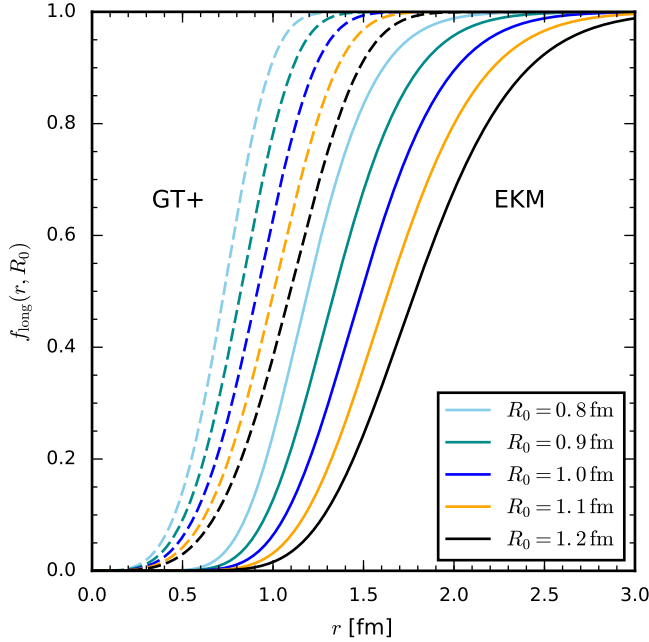


FIG. 2. (Color online) Plot of the long-range regulator functions for the GT+ (dashed) and EKM (solid) potentials with cutoffs $R_0 = 0.8$ – 1.2 fm (see Table I). The regulators corresponding to $R_0^{\text{GT}+} = 1.2$ fm (dashed black line) and $R_0^{\text{EKM}} = 0.8$ fm (solid light blue line) lead to the best agreement.

cut off much slower by the local regulator. This shows that the comparison of the numerical values of R_0 alone can be quite misleading due to the different regulator forms for different interactions.

We can confirm this observation also for the long-range part of the regulators. In Table II we show the distance r^* , where $f_{\text{long}}(r^*, R_0) = 1/2$ for the cutoff range $R_0 = 0.8$ – 1.2 fm. Similarly to the short-range part of the regulators, we find good agreement for $R_0^{\text{GT}+} = 1.2$ fm and $R_0^{\text{EKM}} = 0.8$ fm. As shown in Fig. 2, the regulator functions agree well over the entire range of distances. Therefore, it is natural to expect that the Weinberg eigenvalue analysis will provide similar results for the long-range part for this cutoff combination of these two interactions, which we focus on in Sec. IV.

III. WEINBERG EIGENVALUE ANALYSIS

The Weinberg eigenvalue analysis is a powerful tool to quantify the perturbativeness of nuclear interactions. Perturbativeness is of great importance for most of the many-body frameworks presently used in nuclear physics. On the one hand, the tractability of MBPT directly relies on the rapid convergence of the perturbation series through suppression of higher-order corrections, because otherwise the number of diagrams increases too fast with successive orders. To date, MBPT has been applied to the calculation of the equation of state of infinite nuclear matter up to third order (see, e.g., Refs. [37–43]) and recently to fourth order [44]. In addition, MBPT has been applied to the derivation of valence-space Hamiltonians for open-shell nuclei (see, e.g., Refs. [5, 45]) and recently to the calculation of ground-state energies of closed-shell nuclei [46].

On the other hand, perturbativeness also plays a key role for inherently nonperturbative many-body frameworks that are based on basis expansions such as the no-core-shell model [47], coupled-cluster theory [4], in-medium similarity renormalization group [7], and the self-consistent Green’s function method [48, 49]. For these frameworks, strongly nonperturbative interactions typically require a prohibitively large number of basis states and prevent a reliable extraction of converged results. In recent years, RG methods have been developed in order to improve the perturbativeness of nuclear interactions. However, such RG transformations can generally only be performed approximately and thus lead to additional uncertainties in many-body calculations [50, 51].

We review here briefly the most important aspects of the Weinberg eigenvalue analysis and refer to Ref. [11] for more detailed discussions. To motivate the concept, we consider for simplicity the Lippmann-Schwinger equation for the free-space T -matrix in the center-of-mass frame,

$$T(W) = V + V G_0(W) T(W) \quad (4a)$$

$$= \sum_{n=0}^{\infty} V (G_0(W) V)^n, \quad (4b)$$

with the free propagator $G_0(W) = (W - H_0)^{-1}$, the kinetic energy $H_0 = p^2/m$, where m is the averaged nucleon mass, and W is the complex energy.

Iteration of the Born series (4b) may converge to a self-consistent solution. Due to nonperturbative sources, however, the convergence is by no means guaranteed; e.g., bound states are poles of the T -matrix, which render the expansion naturally divergent. To study convergence and the efficiency of perturbation theory, Weinberg analyzed the eigenvalues of the operator $G_0(W)V$,

$$G_0(W)V |\Psi_\nu(W)\rangle = \eta_\nu(W) |\Psi_\nu(W)\rangle. \quad (5)$$

The so-called Weinberg eigenvalues $\eta_\nu(W)$ are defined in the complex energy plane cut along the positive real axis and form a discrete set for any value of W . In the following, we take $W = E + i\varepsilon$ for positive energies.

Making use of the eigenvalue relation (5), the Born series expansion (4b) is a geometric series which converges if and only if all eigenvalues lie within the unit circle in the complex plane, i.e., $|\eta_\nu(W)| < 1$. The largest eigenvalue sets the rate of convergence, if at all, where overall smaller magnitudes imply faster convergence. When $|\eta_\nu(W)| > 1$, the precise magnitudes of the Weinberg eigenvalues still have a dramatic impact on the convergence in a nonperturbative many-body method.

We summarize here several definitions as well as selected properties of $\eta_\nu(W)$ relevant for this paper. Rewriting the eigenvalue relation (5) as a modified Schrödinger equation [11],

$$\left(H_0 + \frac{V}{\eta_\nu(W)}\right) |\Psi_\nu(W)\rangle = W |\Psi_\nu(W)\rangle, \quad (6)$$

allows intuitively a physical interpretation: the eigenvalue is effectively an energy-depending coupling $\eta_\nu^{-1}(W)$ which rescales the interaction. Following the original discussion by Weinberg, real bound states of the potential having $W = E < 0$ (e.g., for the deuteron, $E = -2.223$ MeV) correspond to $\eta_\nu(E) = 1$. The modified Schrödinger equation corresponds to the physical one in this case. More generally, even though the original potential does not support a bound state with binding energy $E < 0$, a scaled interaction $\eta_\nu^{-1}(E)V$ would have a bound state at E .

A purely attractive potential has only positive eigenvalues for $E < 0$. However, a purely repulsive potential cannot have a bound-state solution of the Schrödinger equation, which naively seems to imply that the modified Schrödinger equation (6) has no solutions. However, (6) may have a solution for a sign-flipped interaction $\eta_\nu^{-1}(E)V$ in which the Weinberg eigenvalue is negative. Therefore, it is convention that a positive (negative) eigenvalue is referred to as an attractive (repulsive) eigenvalue.

In the case of positive energies ($E > 0$) for $W = E + i\varepsilon$ with $\varepsilon \rightarrow 0$, the modified Schrödinger equation has complex energy eigenvalues, leading to complex Weinberg eigenvalues. Thus, we obtain complex (real) eigenvalues for positive (negative) energies E . The same definition of attractive and repulsive as before applies to the imaginary part of the eigenvalues for positive energies, which is motivated by analytic continuation from the solution along the negative real axis. In general, both attractive and repulsive eigenvalues occur for a nuclear potential.

We illustrate the behavior of repulsive and attractive Weinberg eigenvalues in the complex plane for positive energies $E = 0 - 300$ MeV in Figs. 3 and 4, respectively, in the 1S_0 and $^3S_1 - ^3D_1$ channels for a set of three different potentials by taking the limit $\varepsilon \rightarrow 0$ of $\eta_\nu(E + i\varepsilon)$. The trajectories start on the real axis and evolve counterclockwise with increasing energy. Nearly (or shallow) bound states are represented by attractive eigenvalues with magnitudes close to unity for $E = 0$. The deuteron binding energy can be determined by the intersection of the trajectory in the $^3S_1 - ^3D_1$ channel and the unit circle when lowering the energy $E < 0$. Since the attractive eigenvalues are typically dominated by (nearly or shallow)

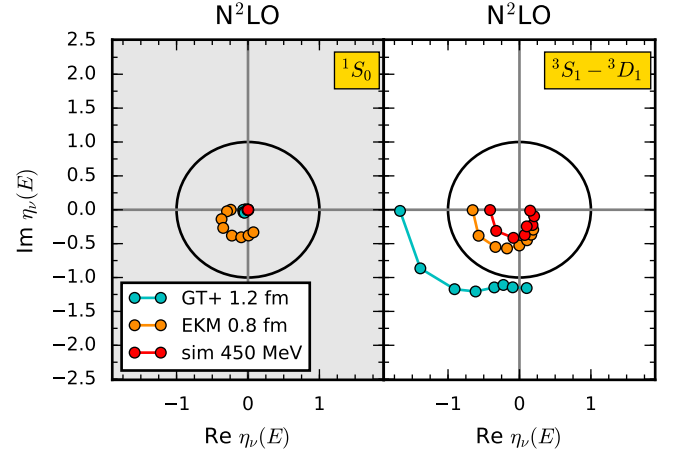


FIG. 3. (Color online) Repulsive Weinberg eigenvalues for the N^2LO NN potentials GT+ 1.2 fm, EKM 0.8 fm, and sim 450 MeV ($T_{\text{rel}} = 290$ MeV) as trajectories of energy in the complex plane, starting on the negative real axes and evolving counterclockwise. We show results for energies $E = 0, 25, 66, 100, 150, 200, 250$, and 300 MeV as circles in the 1S_0 (left panel) and $^3S_1 - ^3D_1$ channels (right panel).

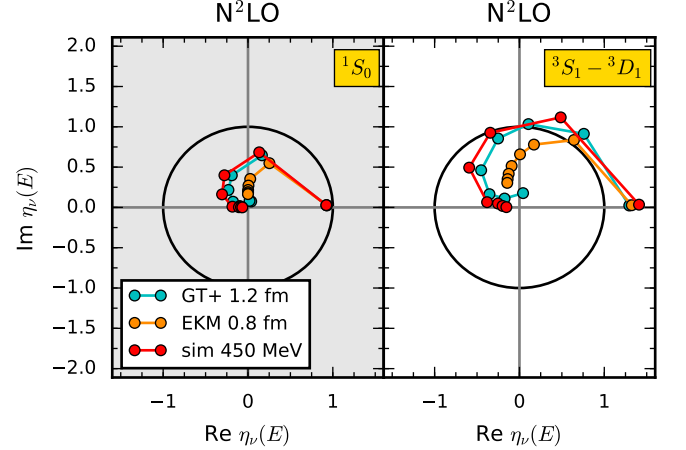


FIG. 4. (Color online) Attractive Weinberg eigenvalues for the N^2LO NN potentials GT+ 1.2 fm, EKM 0.8 fm, and sim 450 MeV ($T_{\text{rel}} = 290$ MeV) as trajectories of energy in the complex plane, starting on the positive real axes and evolving counterclockwise. We show results for energies $E = 0, 25, 66, 100, 150, 200, 250$, and 300 MeV as circles in the 1S_0 (left panel) and $^3S_1 - ^3D_1$ channels (right panel). The (nearly and shallow) bound states close to $E = 0$ are indicated by eigenvalues slightly smaller or larger than 1 in the uncoupled or coupled channel, respectively.

bound states in the two S -wave channels, we discuss in the present paper mainly repulsive eigenvalues.

We also briefly give some details of the calculation. In practice, it is convenient to solve the eigenvalue relation (5) in a partial-wave representation because $G_0V(W)$ is block diagonal in the partial-wave quantum numbers

$(LS)JT$,

$$\begin{matrix} & {}^1S_0 & {}^3S_1 & {}^3D_1 & {}^1P_1 & \dots \\ \begin{matrix} {}^1S_0 \\ {}^3S_1 \\ {}^3D_1 \\ {}^1P_1 \\ \vdots \end{matrix} & \begin{pmatrix} \blacksquare & 0 & 0 & 0 & \dots \\ 0 & \blacksquare & \blacksquare & 0 & \dots \\ 0 & \blacksquare & \blacksquare & 0 & \dots \\ 0 & 0 & 0 & \blacksquare & \dots \\ \vdots & \vdots & \vdots & \vdots & \ddots \end{pmatrix} \end{matrix}, \quad (7)$$

where L denotes the angular momentum, S the two-body spin, J the total angular momentum, and T the two-body isospin. This allows one to separately diagonalize blocks of given S , J , and T (the \blacksquare in Eq. (7)),

$$\begin{aligned} \frac{2}{\pi} \sum_{L,L'} \int dk' \frac{k'^2 m V_{LL'S}^{JT}(k, k')}{k_0^2 - k'^2 + i\varepsilon} \langle k'(L'S)JT | \Psi_\nu(W) \rangle \\ = \eta_\nu(W) \sum_L \langle k(LS)JT | \Psi_\nu(W) \rangle, \end{aligned} \quad (8)$$

where different L values may be coupled due to the potential ($k_0^2 + i\varepsilon = mW$). For coupled channels, we have $L, L' = |J \pm 1|$, whereas in uncoupled channels $L = L'$. The main discussion of this paper is based on the free propagator and on the neutron-proton (np) channel but isospin-symmetry breaking is usually small. Hence, we have dropped the index $M_T = 0$ for simplicity.

In the case of negative energies (i.e., purely imaginary k_0), poles do not occur and we can take $\varepsilon = 0$. Technically, we then solve the eigenvalue problem on a well-suited Gaussian quadrature momentum grid to ensure numerical convergence. After performing the standard substitution $\int dp \rightarrow \sum_{i=1}^{N_p}$, the left-hand side of the eigenvalue problem (8) can be written as a matrix. The basis vectors have a size of N_p ($2N_p$) in an uncoupled (coupled) channel.

For the positive energies, however, one has to carefully take into account the pole in Eq. (8) at $k = k_0$. In that case, we make use of the Sokhotski-Plemelj theorem for a real, continuous function $f(k)$,

$$\frac{f(k)}{k - (k_0 \pm i\varepsilon)} = \mathcal{P} \frac{f(k)}{k - k_0} \pm i\pi \delta(k - k_0) f(k), \quad (9)$$

with the Cauchy principal value \mathcal{P} , and integrate explicitly over the singularity. Following Ref. [52], we convert the principal-value integral into a standard integral by adding

$$-g(k_0) \mathcal{P} \int_0^\infty \frac{dk}{k^2 - k_0^2} = 0 \quad (10)$$

to Eq. (8) in order to make the integral well behaved, i.e.,

$$\mathcal{P} \int_0^\infty dk \frac{g(k)}{k^2 - k_0^2} = \int_0^\infty dk \frac{g(k) - g(k_0)}{k^2 - k_0^2}, \quad (11)$$

where we define $f(k) = g(k)/(k + k_0)$. To evaluate numerically the integral on the right-hand side of Eq. (11), it is crucial to split the integral at some sufficiently large $p_{\max} > k_0$ such that $f(k)$ is known to vanish for all

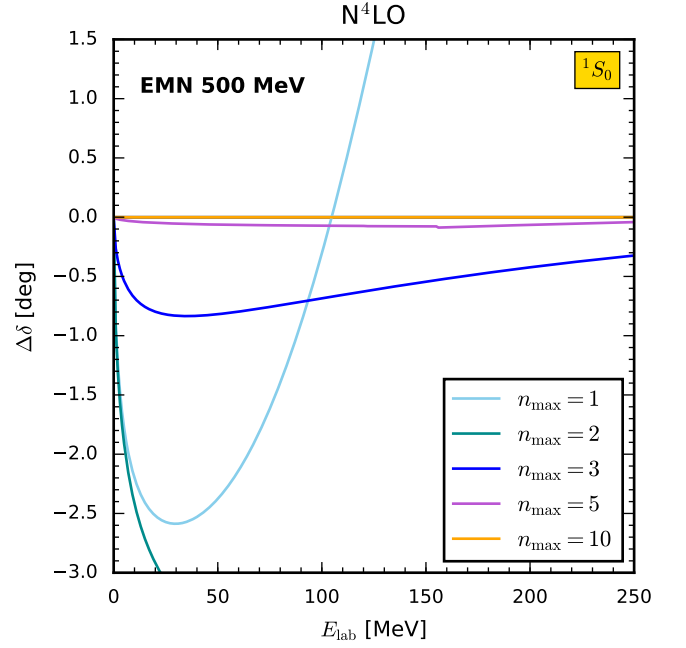


FIG. 5. (Color online) Convergence pattern of 1S_0 phase shifts calculated using the largest Weinberg eigenvalues and different truncations $n \leq n_{\max}$ in expansion (13). The results are based on the 500 MeV EMN potential at $N^4\text{LO}$, but the other potentials and channels show a similar behavior, and the phase shifts are plotted as a function of $E_{\text{lab}} = 2E$. Note that for $n_{\max} = 1$, we restrict the sum to the largest attractive (instead of the overall largest) eigenvalue to avoid a discontinuity that happens because the trajectories of attractive and repulsive eigenvalues are crossing each other.

$p > p_{\max}$. Because of the regularization of the potential, it is usually straightforward to find a suitable value for p_{\max} . The advantage of this procedure is that the remaining integral of the form

$$\int_{p_{\max}}^\infty \frac{dk}{k^2 - k_0^2} = \frac{1}{k_0} \text{artanh} \left(\frac{k_0}{p_{\max}} \right) \quad (12)$$

no longer has a pole because of $p_{\max} > k_0$, and can be evaluated analytically. We have carefully checked the numerical stability of this method, in particular the subtraction in Eq. (11). The subtracted pole as well as the additional constant term in Eq. (9) are taken care of by enlarging the basis vector by one for each L component, so the matrix to be diagonalized is of rank $N_p + 1$ ($2N_p + 2$) for an uncoupled (coupled) channel.

Finally, we review an intriguing feature of the Weinberg analysis. Weinberg showed in Section VI of Ref. [11] that the eigenvalues and phase shifts in an uncoupled channel $(LS)JT$ are related by

$$\delta_{LS}^{JT}(E) = \sum_{\nu=1}^{\infty} \delta_\nu(E), \quad (13)$$

with the so-called elemental phase shifts defined as

$$\delta_\nu(E) \equiv -\arg(1 - \eta_\nu(E + i\varepsilon)), \quad (14)$$

where the η_ν are solutions to Eq. (8) for the uncoupled channel. For coupled channels, Eq. (13) leads to the sum of the partial phase shifts, $\delta_{L-1S}^{JT} + \delta_{L+1S}^{JT}$, which is independent of a particular phase-shift convention. Repulsive (attractive) eigenvalues lead to elemental phase shifts in $[-\pi, 0]$ ($[0, \pi]$) resulting, as expected for purely repulsive (attractive) interactions, in negative (positive) phase shifts.

Weinberg already observed that Eq. (13) usually converges rapidly, taking into account only a few terms. Consequently, there can only be a few eigenvalues with significant magnitudes. We find a similar convergence pattern also for our representative set of modern chiral potentials. In Fig. 5, we show the residuals

$$\Delta\delta_{LS}^{JT}(E) = \sum_{\nu=1}^{n_{\max}} \delta_\nu(E) - \delta_{LS}^{JT}(E), \quad (15)$$

evaluated for several truncations n_{\max} . The results in Fig. 5 are shown for the 500 MeV EMN potential at N⁴LO in the ¹S₀ channel; however, the other potentials and channels discussed in this paper behave similarly. The reference phase shifts $\delta_{LS}^{JT}(E)$ result from the on-shell T matrix as obtained in a nonperturbative calculation by inverting Eq. (4a). The converged phase shifts are very well reproduced for $n_{\max} \sim 5 - 10$.

IV. RESULTS

In this section, we apply the Weinberg eigenvalue analysis to the recent local, semilocal, and nonlocal chiral potentials in different partial waves. We investigate and compare characteristic features of each potential order by order and exploit the regulator comparison of Sec. II for the local and semilocal potentials. The repulsive eigenvalues manifest the differences between the various potentials, so we focus our analysis on them, but also illustrate the common trends of attractive eigenvalues. At the end we revisit the question of whether distinct but phase-equivalent initial potentials flow to the same low-momentum form under the similarity RG.

We start with the ¹S₀ and coupled ³S₁–³D₁ channels, as they are most important for low-energy physics, and then extend the discussion to higher partial waves. In Figs. 6 and 7, we show the magnitude of the S -wave repulsive eigenvalues as a function of energy from leading order (LO) up to the highest order available, respectively, for the local GT+, semilocal EKM, and nonlocal EMN potentials in each row with various cutoffs. The dotted black line denotes where the Born series expansion diverges, corresponding to the unit circle in Figs. 3 and 4. For the GT+ potential we use the SFR cutoff $\tilde{\Lambda} = 1000$ MeV. From these figures, we observe the following:

- In the ¹S₀ channel, all three LO potentials are purely attractive and so the repulsive eigenvalues are zero. In contrast, the corresponding eigenvalues in the

³S₁–³D₁ channel are nonzero and show significant differences, with the EKM potentials softer than GT+ and EMN.

- At NLO we find nonvanishing repulsive eigenvalues, large in magnitude for the GT+ potential and even larger for the EMN potential in the ¹S₀ channel. In the ³S₁–³D₁ channel we observe magnitudes up to 8 for the GT+ 0.9 fm potential and up to 2.5 for the EMN 550 MeV potential, while eigenvalues are below 1 for the EKM potential in both channels.
- Going from NLO to N²LO leads to reduced eigenvalues uniformly, with EMN in particular going from nonperturbative for the larger Λ values to perturbative.
- The eigenvalues for the EKM and EMN potentials in the ¹S₀ channel jump upwards at N³LO and stay equally large in magnitude at N⁴LO. In the ³S₁–³D₁ channel, the eigenvalues for the EKM potential again increase at N³LO and N⁴LO, whereas for the EMN potential we observe essentially no change in magnitude but an increased spread in Λ for higher energies. Enhanced repulsive eigenvalues at N³LO were discussed in Ref. [17] due to the sub-sub-leading two-pion exchange as a new nonperturbative source entering at N³LO. It is interesting to note that these jumps in the eigenvalues are also manifested in the form of large energy changes of the triton binding energy [10, 53] based on these two-body interactions [54].

All potentials at all orders get softened for larger coordinate-space cutoffs or smaller momentum-space cutoffs, respectively, resulting in less repulsion and therefore smaller repulsive eigenvalues. In general, the larger eigenvalues of the local GT+ potentials indicate that it is less perturbative than the semilocal or nonlocal potentials. This observation is consistent with past studies of local versus nonlocal one-boson-exchange potentials [55]. However, as discussed in Sec. II, a direct comparison of the local GT+ and semilocal EKM potentials with the same regulator parameter R_0 is misleading because of the differing forms of the regulator functions. We identified comparable cutoff values, but good agreement for eigenvalues of the corresponding full potentials is only seen at LO. In Fig. 8 we compare the full and contactless potentials to shed light on the deviations. In this context, contactless means all contacts up to the given chiral order are set to zero. We find fair agreement for eigenvalues of the contactless potentials in both channels, even at NLO and N²LO. Thus we conclude that the different inclusion of the momentum-dependent short-range couplings (for local, and semilocal or nonlocal) at NLO and beyond lead to the differences in eigenvalues.

We also examined the S -wave repulsive eigenvalues for selected nonlocal N²LO sim potentials, which are shown in Fig. 9. They are similar to the EKM and EMN results in the ¹S₀ channel, while in the ³S₁–³D₁ channel the

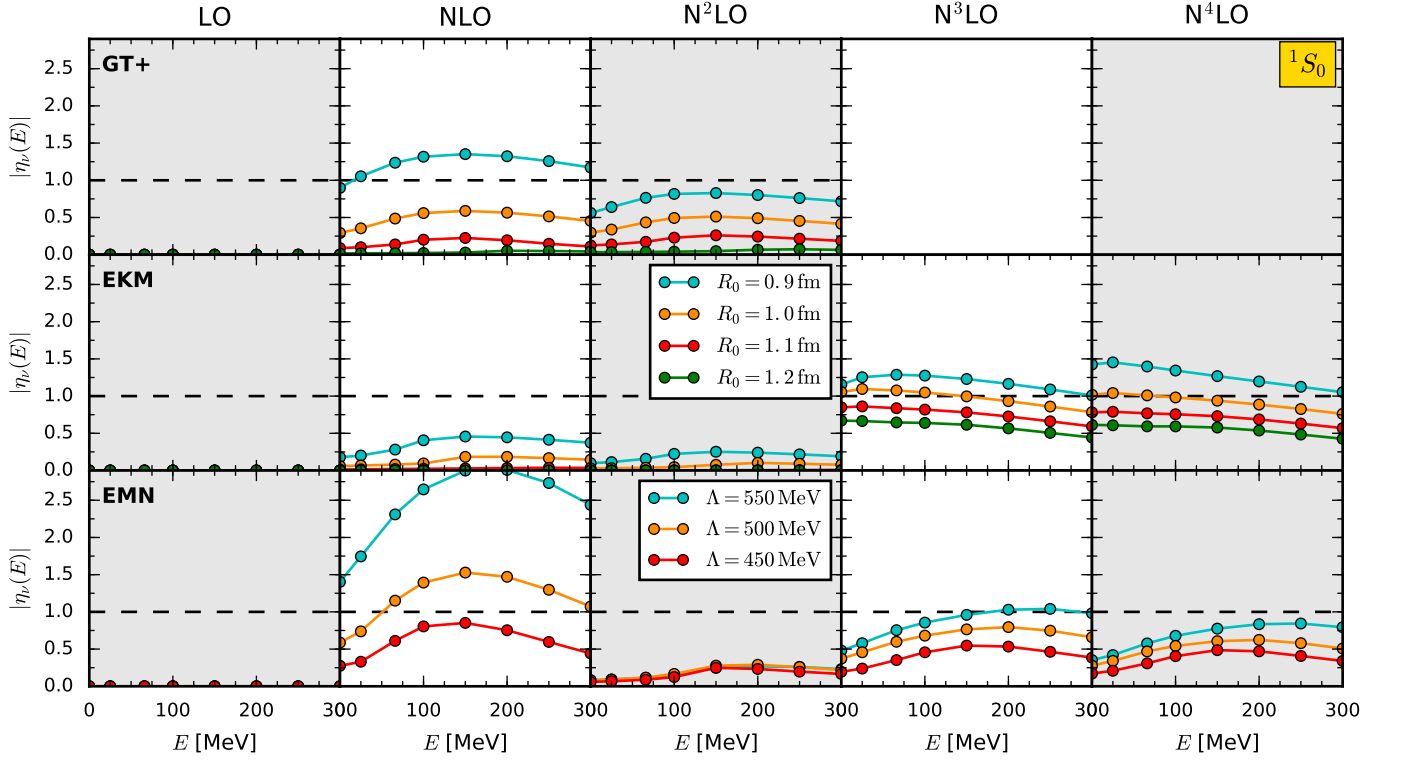


FIG. 6. (Color online) Magnitude of the repulsive Weinberg eigenvalues for the GT+ (first row), EKM (middle row), and EMN potentials (bottom row) as a function of energy $E = 0, 25, 66, 100, 150, 200, 250$, and 300 MeV in the 1S_0 channel up to the highest chiral order available, respectively. We show results for coordinate-space cutoffs $R_0 = 0.9 - 1.2$ fm for the GT+ and EKM potentials, as well as for momentum-space cutoffs $\Lambda = 450 - 550$ MeV for the EMN potential.

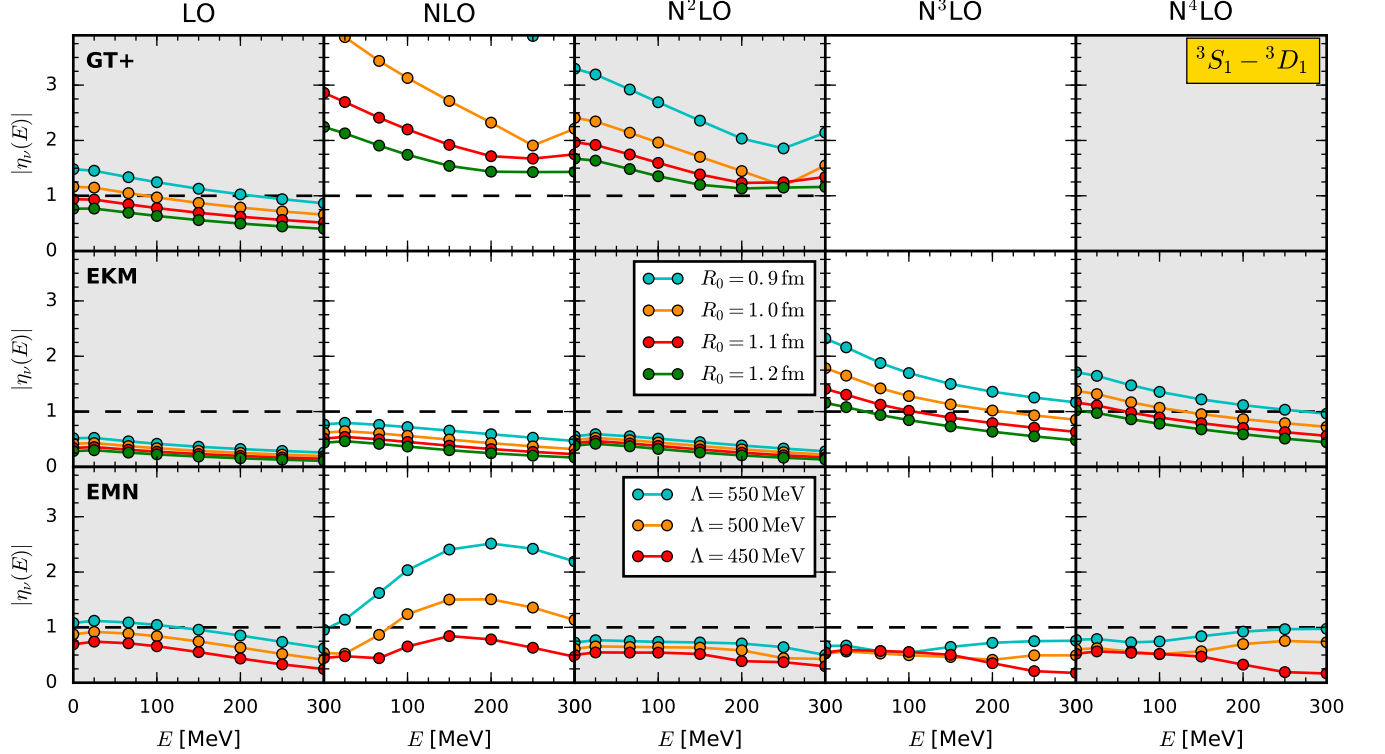


FIG. 7. (Color online) Same as Fig. 6 but for the $^3S_1 - ^3D_1$ channel. Notice that the Weinberg eigenvalues are above the scale for the NLO NN potential GT+ 0.9 fm, as we use the same plot range for all panels for better comparison.

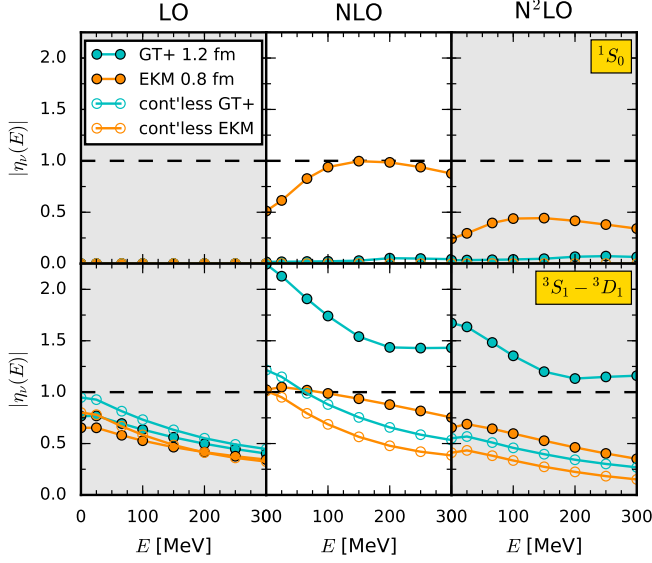


FIG. 8. (Color online) Magnitude of the repulsive Weinberg eigenvalues for the GT+ and EKM potential for the fixed cutoff combination derived in Sec. II, at LO, NLO, and N²LO. We show results for the full potential (solid circles) in contrast to the potential without contacts (open circles) in the 1S_0 (upper panel) and $^3S_1-^3D_1$ channels (lower panel). The eigenvalues for the contactless potential are in fair agreement for the cutoff combination $R_0^{GT+} = 1.2$ fm and $R_0^{EKM} = 0.8$ fm at all orders and in both channels.

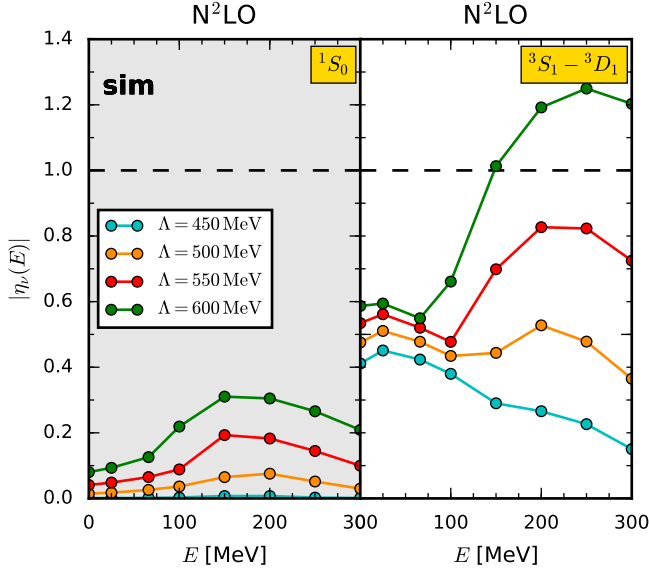


FIG. 9. (Color online) Magnitude of the repulsive Weinberg eigenvalues for the N²LO sim potential with $T_{\text{rel}} = 290$ MeV and the cutoff range $\Lambda = 450 - 600$ MeV as a function of energy $E = 0, 25, 66, 100, 150, 200, 250$, and 300 MeV in the 1S_0 (left panel) and $^3S_1-^3D_1$ channels (right panel).

eigenvalues show a spread in Λ as for the N²LO EMN potential. In addition, the pattern of energy dependence is different except for the softest cutoff.

Examples of repulsive eigenvalues in the higher partial waves for the EMN and EKM potentials are shown in Figs. 10 and 11, respectively. In most channels there are not significant differences. The increases going from N²LO to N³LO noted for the S waves are present for the EKM P waves but without the dramatic jumps. These are only seen for the EMN potential in the 3D_2 channel. The energy dependence of the repulsive eigenvalues is generally similar even for different regulators. However, as noted, the N²LO sim potential shows quite different energy dependence in the $^3S_1-^3D_1$ channel as the cutoff increases.

The attractive eigenvalues in the 1S_0 and $^3S_1-^3D_1$ channels are shown in Figs. 12 and 13, respectively, for the GT+, EKM, and EMN potentials. We find only minor dependence on the cutoff and nearly the same eigenvalues for all potentials at all chiral orders. This behavior follows because the magnitude of the attractive eigenvalues is determined by the shallow or nearly bound state to be close to 1 at low energies. The energy dependence for all potentials at all orders and in both channels shows the same fall-off toward perturbative values.

These many observations illustrate how Weinberg eigenvalues may point to subtle issues, e.g., with the fitting procedure, but following up in detail is beyond the scope of this paper. Instead we give examples of more general conclusions from consideration of the eigenvalue systematics:

- For the EKM potential, we traced the increased eigenvalues at N³LO and N⁴LO to the new contacts at N³LO. We observe eigenvalues equal to zero for the potential without N³LO contacts in the 1S_0 channel, and significantly reduced eigenvalues (below 1) in the $^3S_1-^3D_1$ channel. We conclude that the main contribution to the change in magnitude is from the contacts at this order.
- The repulsion needed to obtain correct phase shifts at high energies is provided by contact terms, but how this is realized differs between local and non-local implementations. For local potentials, the repulsive part is largely built up through the energy-independent LECs, because the q^2 -dependent contacts at NLO and beyond are suppressed by at least a factor r^2 in coordinate space. This LEC contributes equally at lower energies, leading to enhanced eigenvalues at NLO and beyond. The buildup of the short-range repulsion is visible in Fig. 14 for the N²LO GT+ potential in coordinate space. In contrast, contact terms for the semilocal and nonlocal potentials at NLO and beyond also depend on k^2 , which allows for momentum dependence, with large (small) repulsion for higher (lower) energies. Here, $\mathbf{k} = (\mathbf{p} + \mathbf{p}')/2$ is the momentum transfer in the exchange channel.
- We observed reduced eigenvalues when going from NLO to N²LO. This could be due to the improved

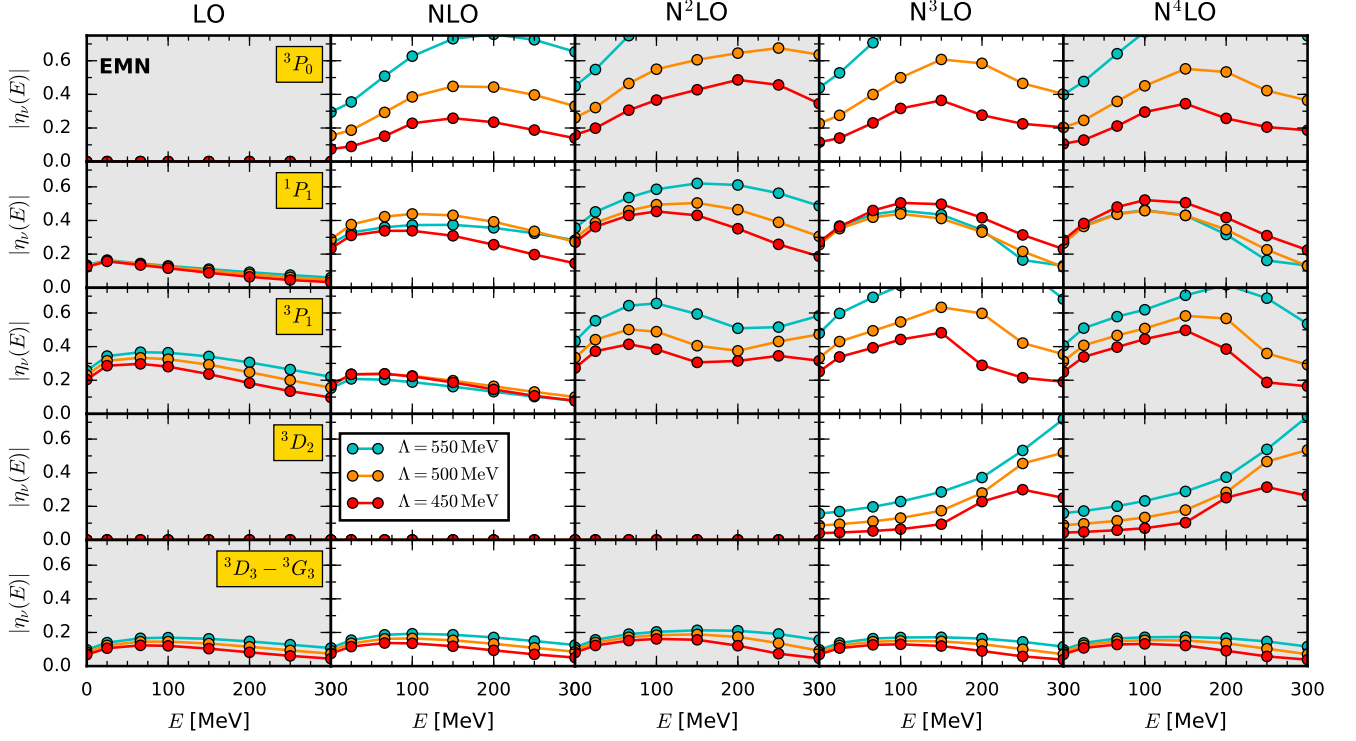


FIG. 10. (Color online) Magnitude of the repulsive Weinberg eigenvalues for the EMN potential up to $N^4\text{LO}$ as a function of energy $E = 0, 25, 66, 100, 150, 200, 250$, and 300 MeV in different higher partial waves. We show results for momentum-space cutoffs $\Lambda = 450 - 550$ MeV. Notice that some eigenvalues are partially above the scale, as we apply the same plot range at all chiral orders and partial waves for better comparison.

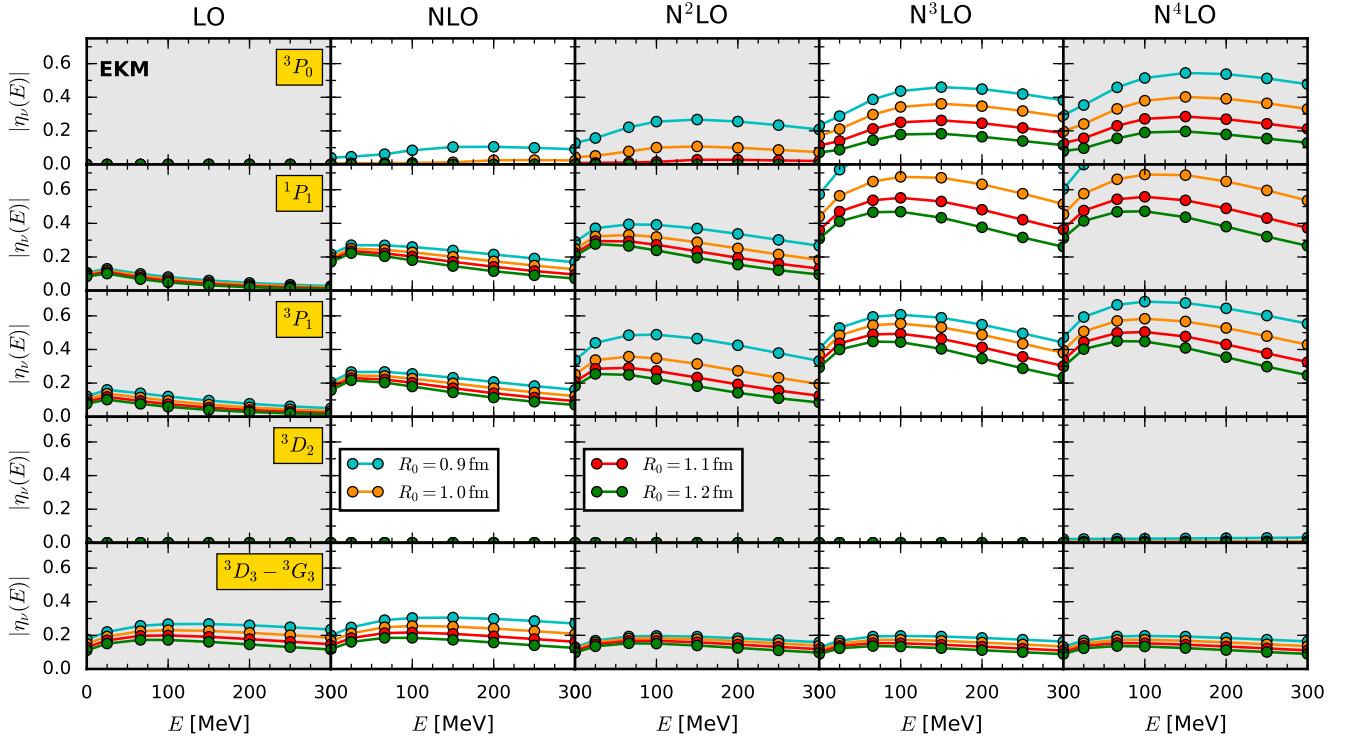


FIG. 11. (Color online) Magnitude of the repulsive Weinberg eigenvalues for the EKM potential up to $N^4\text{LO}$ as a function of energy $E = 0, 25, 66, 100, 150, 200, 250$, and 300 MeV in different higher partial waves. We show results for coordinate-space cutoffs $R_0 = 0.9 - 1.2$ fm.

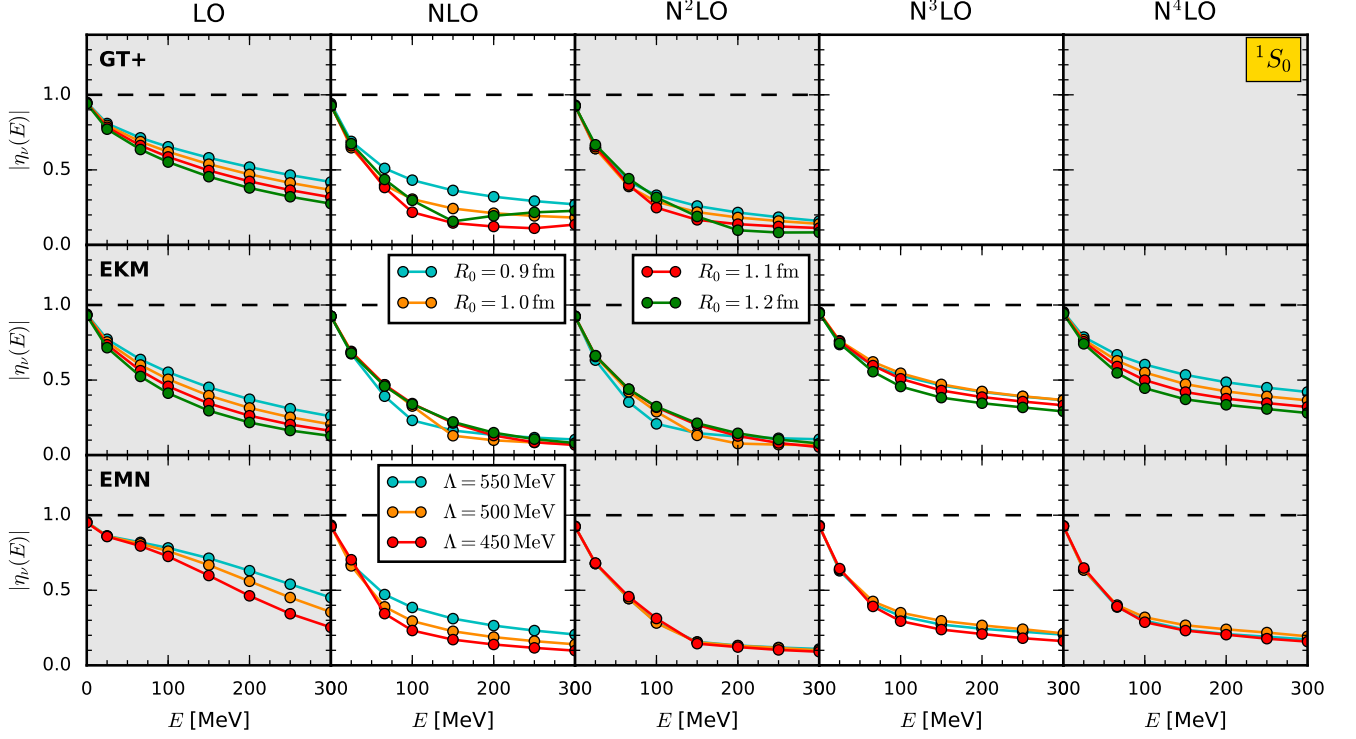


FIG. 12. (Color online) Magnitude of the attractive Weinberg eigenvalues for the GT+ (first row), EKM (middle row), and EMN potentials (bottom row), as a function of energy $E = 0, 25, 66, 100, 150, 200, 250$, and 300 MeV in the 1S_0 channel up to the highest chiral order available, respectively. We show results for coordinate-space cutoffs $R_0 = 0.9 - 1.2$ fm for the GT+ and EKM potential, as well as for momentum-space cutoffs $\Lambda = 450 - 550$ MeV for the EMN potential.

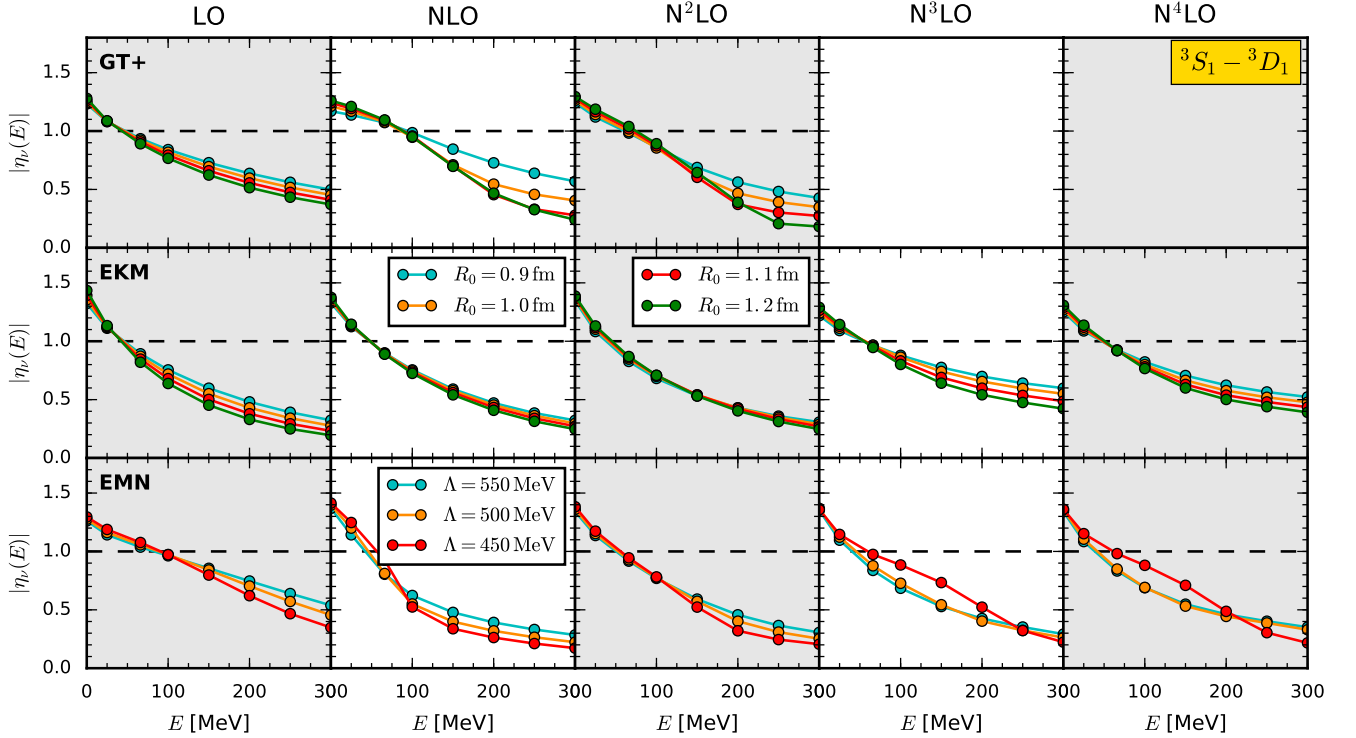


FIG. 13. (Color online) Same as Fig. 12 but for the $^3S_1 - ^3D_1$ channel.

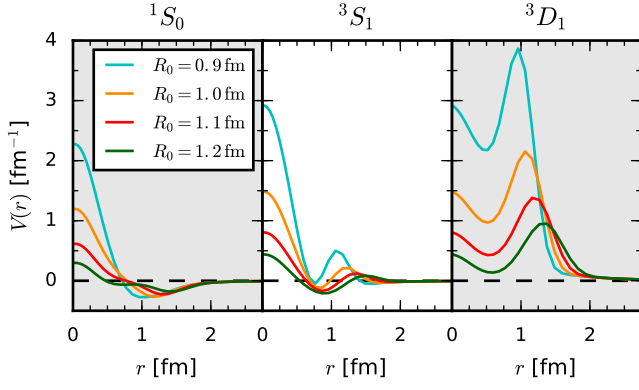


FIG. 14. (Color online) Coordinate-space representation of the GT+ potential at N²LO for the cutoff range $R_0 = 0.9–1.2$ fm in the 1S_0 (left), 3S_1 (middle), and 3D_1 (right) channels.

description of the midrange part of the potential as a result of the subleading two-pion exchange, entering at N²LO, which requires less fitting into the contact parameters at this order.

- While one might have guessed that the enhanced repulsive Weinberg eigenvalues are due to the low- to high-momentum coupling of local regulators, this is actually not the case. This has been verified by adding an additional sharp cutoff of $\Lambda = 4–5$ fm^{−1}, which leaves the eigenvalues nearly unchanged, showing that they are determined by the contributions below this cutoff.

In general, even when comparing regulators for different potentials can be quite cumbersome, the Weinberg eigenvalue analysis as a diagnostic tool offers the possibility to study the perturbativeness, indicate scheme dependence and possible issues in the fitting procedure, as well as draw conclusions on the regulator impact.

For a given family of potentials, defined with the same regularization scheme and constructed with the same fitting protocol, the repulsive Weinberg eigenvalues reflect the softening of the interaction with progressively smaller (larger) regulator parameters in momentum (coordinate) space. This softening can also be realized through an RG evolution, e.g., via the similarity RG (SRG). In Fig. 15 we show the eigenvalues at zero energy in the 1S_0 and $^3S_1–^3D_1$ channel at N²LO for the EKM, EMN, and GT+ potentials, as well as at N³LO for the EKM and EMN potentials as a function of the SRG parameter λ . The eigenvalues at large λ , which correspond to the unevolved (initial) potentials, exhibit the dramatic jump in hardness from 1S_0 to $^3S_1–^3D_1$ for GT+, and in both channels from N²LO to N³LO for EKM. The jump is much smaller for EMN 1S_0 and no change or even a softening is observed for EMN $^3S_1–^3D_1$. With evolution to smaller λ , all potentials are monotonically softened, with even the EKM N³LO and GT+ N²LO $^3S_1–^3D_1$ eigenvalues becoming perturbative for $\lambda < 4$ fm^{−1}, and $\lambda < 3.5$ fm^{−1}, respectively.

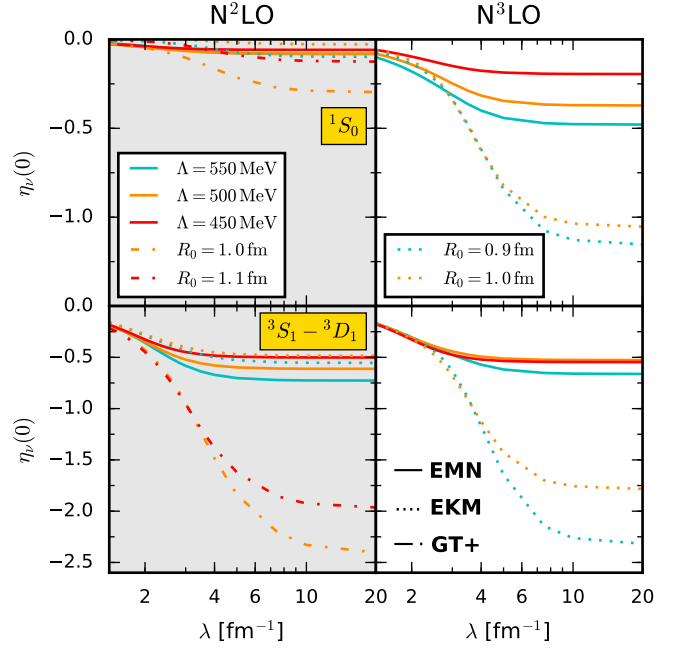


FIG. 15. (Color online) Repulsive Weinberg eigenvalues for the N²LO EMN (solid lines), EKM (dotted lines), and GT+ (dash-dotted lines) and N³LO EMN (solid lines) and EKM (dotted lines) NN potentials at $E = 0$ as a function of the SRG resolution scale λ in the 1S_0 (upper panels) and the $^3S_1–^3D_1$ channels (lower panels). For small λ , the eigenvalues are in good agreement and exhibit the universality for potentials evolved to low resolution scales.

The fine details of the eigenvalue flow mirror the flow of the potential matrix elements. In Figs. 16 and 17 we show the unevolved and SRG-evolved diagonal and off-diagonal matrix elements in the 1S_0 channel for the EMN, EKM, and GT+ potentials at N²LO, as well as the EMN and EKM potentials at N³LO, respectively, as functions of the momentum. At N²LO, the relatively small degree of softening reflects the suppression of off-diagonal matrix elements, and all matrix elements are quantitatively close for $\lambda = 2$ fm^{−1}. At N³LO, both diagonal and off-diagonal matrix elements exhibit a flow toward universal potentials for momenta below λ .

V. SUMMARY AND OUTLOOK

In this paper we performed a comprehensive Weinberg eigenvalue analysis of a representative set of modern NN interactions derived within chiral EFT. Our results provide insights into the perturbativeness and scheme dependencies of these interactions.

We find that the attractive eigenvalues, determined by the shallow or nearly bound states in the 1S_0 and $^3S_1–^3D_1$ channels, show a universal behavior for all investigated potentials at all orders in the chiral expansion. In contrast, the repulsive eigenvalues depend on specific details such as the regularization scheme, in particular for

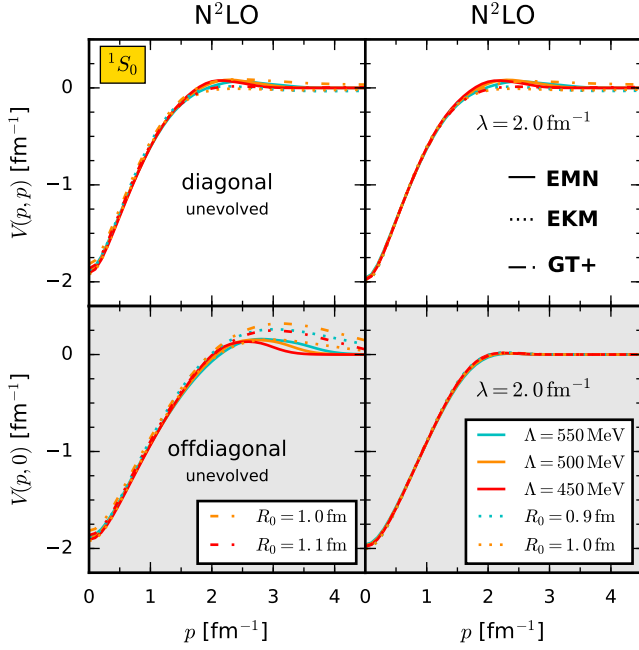


FIG. 16. (Color online) Diagonal (upper row) and offdiagonal (lower row) matrix elements $V(p, p' = p)$, $V(p, p' = 0)$, respectively, of the unevolved (left column) and SRG evolved to $\lambda = 2.0 \text{ fm}^{-1}$ (right column) $N^2\text{LO}$ potentials of EMN (solid lines), EKM (dotted lines), and GT+ (dash-dotted lines) in momentum space in the 1S_0 channel. For small λ the diagonal elements of all potentials are again in good agreement.

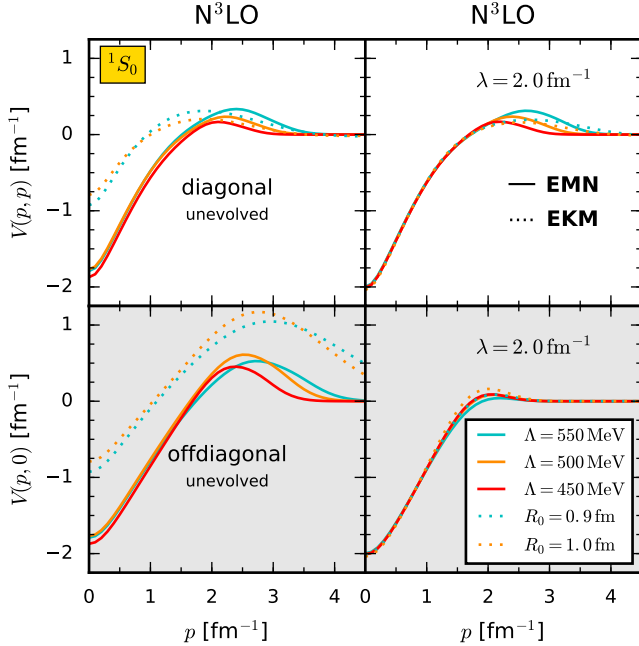


FIG. 17. (Color online) Same as Fig. 16 but for the EMN and EKM potentials at $N^3\text{LO}$.

the short-range parts of the interaction. This means that the eigenvalues at different orders in the chiral expansion for a given class of interactions can behave quite differ-

ently. While the GT+ potentials develop large repulsive eigenvalues from LO to NLO, the EKM potentials remain perturbative up to $N^2\text{LO}$ and become nonperturbative only at $N^3\text{LO}$ and $N^4\text{LO}$. We can trace back this sudden increase at $N^3\text{LO}$ to the presence of new short-range couplings at this order. In comparison, the investigated nonlocal potentials EMN and sim tend to remain more perturbative at all orders.

Moreover, we found that a direct comparison of coordinate-space cutoff values for the GT+ and EKM interactions can be quite misleading due to different functional forms of the employed regulators. For example, we find that a cutoff of $R_0^{\text{GT}+} = 1.2 \text{ fm}$ essentially corresponds to $R_0^{\text{EKM}} \approx 0.8 \text{ fm}$. This highlights that direct comparisons of regulator parameters are not warranted; alternative ways to compare are given in Sec. II. Finally, we examined the flow to universality of Weinberg eigenvalues and interaction matrix elements for the GT+, EKM, and EMN potentials under SRG evolution.

In future work, our analysis can be directly extended to study regulator artifacts at finite density via in-medium eigenvalues and to include 3N interactions to assess their impact on perturbativeness. Furthermore, a comparison of potentials containing delta resonances to delta-less potentials, which are expected to have different order-by-order convergence patterns, would be illuminating. The applications shown in this paper, including the relation to phase shifts, suggest that Weinberg eigenvalues can serve as a useful feedback in fitting potentials by pointing to subtle issues in the fitting procedure and offering a tool to assess alternative regulator choices.

ACKNOWLEDGMENTS

We thank J. E. Lynn, R. Machleidt, I. Tews, and S. Wesolowski for useful discussions, and R. Machleidt also for providing us with the EMN potentials. C.D. thanks the OSU theory group for the warm hospitality. This work was supported in part by the European Research Council Grant No. 307986 STRONGINT, the Deutsche Forschungsgemeinschaft through Grant SFB 1245, the U.S. National Science Foundation under Grant No. PHY-1614460, and the NUCLEI SciDAC Collaboration under U.S. Department of Energy Grant DE-SC0008533. Computational resources have been provided by the Lichtenberg high performance computer of the TU Darmstadt.

-
- [1] E. Epelbaum, H.-W. Hammer, and U.-G. Meißner, *Rev. Mod. Phys.* **81**, 1773 (2009).
- [2] R. Machleidt and D. R. Entem, *Phys. Rep.* **503**, 1 (2011).
- [3] D. R. Entem and R. Machleidt, *Phys. Rev. C* **68**, 041001(R) (2003).
- [4] G. Hagen, T. Papenbrock, M. Hjorth-Jensen, and D. J. Dean, *Rep. Prog. Phys.* **77**, 096302 (2014).
- [5] K. Hebeler, J. D. Holt, J. Menéndez, and A. Schwenk, *Ann. Rev. Nucl. Part. Sci.* **65**, 457 (2015).
- [6] G. Hagen, A. Ekström, C. Forssén, G. R. Jansen, W. Nazarewicz, T. Papenbrock, K. A. Wendt, S. Bacca, N. Barnea, B. Carlsson, C. Drischler, K. Hebeler, M. Hjorth-Jensen, M. Miorelli, G. Orlandini, A. Schwenk, and J. Simonis, *Nature Phys.* **12**, 186 (2016).
- [7] H. Hergert, S. K. Bogner, T. D. Morris, A. Schwenk, and K. Tsukiyama, *Phys. Rep.* **621**, 165 (2016).
- [8] D. R. Entem, N. Kaiser, R. Machleidt, and Y. Nosyk, *Phys. Rev. C* **91**, 014002 (2015).
- [9] E. Epelbaum, H. Krebs, and U.-G. Meißner, *Phys. Rev. Lett.* **115**, 122301 (2015).
- [10] D. R. Entem, R. Machleidt, and Y. Nosyk, *Phys. Rev. C* **96**, 024004 (2017).
- [11] S. Weinberg, *Phys. Rev.* **131**, 440 (1963).
- [12] R. Jost and A. Pais, *Phys. Rev.* **82**, 840 (1951).
- [13] W. Kohn, *Rev. Mod. Phys.* **26**, 292 (1954).
- [14] K. Meetz, *J. Math. Phys.* **3**, 690 (1962).
- [15] S. Weinberg, *Phys. Rev.* **130**, 776 (1963).
- [16] S. K. Bogner, A. Schwenk, R. J. Furnstahl, and A. Nogga, *Nucl. Phys. A* **763**, 59 (2005).
- [17] S. K. Bogner, R. J. Furnstahl, S. Ramanan, and A. Schwenk, *Nucl. Phys. A* **773**, 203 (2006).
- [18] S. Ramanan, S. K. Bogner, and R. J. Furnstahl, *Nucl. Phys. A* **797**, 81 (2007).
- [19] S. Ramanan and M. Urban, *Phys. Rev. C* **88**, 054315 (2013).
- [20] R. Navarro Pérez, J. E. Amaro, and E. Ruiz Arriola, *Phys. Rev. C* **91**, 054002 (2015).
- [21] S. Srinivas and S. Ramanan, *Phys. Rev. C* **94**, 064303 (2016).
- [22] A. Gezerlis, I. Tews, E. Epelbaum, S. Gandolfi, K. Hebeler, A. Nogga, and A. Schwenk, *Phys. Rev. Lett.* **111**, 032501 (2013).
- [23] A. Gezerlis, I. Tews, E. Epelbaum, M. Freunek, S. Gandolfi, K. Hebeler, A. Nogga, and A. Schwenk, *Phys. Rev. C* **90**, 054323 (2014).
- [24] E. Epelbaum, H. Krebs, and U.-G. Meißner, *Eur. Phys. J. A* **51**, 53 (2015).
- [25] B. D. Carlsson, A. Ekström, C. Forssén, D. F. Strömberg, G. R. Jansen, O. Lilja, M. Lindby, B. A. Mattsson, and K. A. Wendt, *Phys. Rev. X* **6**, 011019 (2016).
- [26] E. Epelbaum, W. Glöckle, and U.-G. Meißner, *Nucl. Phys. A* **747**, 362 (2005).
- [27] V. G. J. Stoks, R. A. M. Klomp, M. C. M. Rentmeester, and J. J. de Swart, *Phys. Rev. C* **48**, 792 (1993).
- [28] M. Hoferichter, J. Ruiz de Elvira, B. Kubis, and U.-G. Meißner, *Phys. Rev. Lett.* **115**, 192301 (2015).
- [29] J. R. Bergervoet, P. C. van Campen, W. A. van der Sanden, and J. J. de Swart, *Phys. Rev. C* **38**, 15 (1988).
- [30] M. Piarulli, L. Girlanda, R. Schiavilla, R. Navarro Pérez, J. E. Amaro, and E. Ruiz Arriola, *Phys. Rev. C* **91**, 024003 (2015).
- [31] M. Piarulli, L. Girlanda, R. Schiavilla, A. Kievsky, A. Lovato, L. E. Marcucci, S. C. Pieper, M. Viviani, and R. B. Wiringa, *Phys. Rev. C* **94**, 054007 (2016).
- [32] A. Ekström, G. Hagen, T. D. Morris, T. Papenbrock, and P. D. Schwartz, [arXiv:1707.09028](https://arxiv.org/abs/1707.09028).
- [33] J. E. Lynn, J. Carlson, E. Epelbaum, S. Gandolfi, A. Gezerlis, and A. Schwenk, *Phys. Rev. Lett.* **113**, 192501 (2014).
- [34] I. Tews, S. Gandolfi, A. Gezerlis, and A. Schwenk, *Phys. Rev. C* **93**, 024305 (2016).
- [35] J. E. Lynn, I. Tews, J. Carlson, S. Gandolfi, A. Gezerlis, K. E. Schmidt, and A. Schwenk, *Phys. Rev. Lett.* **116**, 062501 (2016).
- [36] J. E. Lynn, I. Tews, J. Carlson, S. Gandolfi, A. Gezerlis, K. E. Schmidt, and A. Schwenk, *Phys. Rev. C* **96**, 054007 (2017).
- [37] K. Hebeler, S. K. Bogner, R. J. Furnstahl, A. Nogga, and A. Schwenk, *Phys. Rev. C* **83**, 031301(R) (2011).
- [38] I. Tews, T. Krüger, K. Hebeler, and A. Schwenk, *Phys. Rev. Lett.* **110**, 032504 (2013).
- [39] L. Coraggio, J. W. Holt, N. Itaco, R. Machleidt, L. E. Marcucci, and F. Sammarruca, *Phys. Rev. C* **89**, 044321 (2014).
- [40] C. Wellenhofer, J. W. Holt, and N. Kaiser, *Phys. Rev. C* **93**, 055802 (2016).
- [41] C. Drischler, K. Hebeler, and A. Schwenk, *Phys. Rev. C* **93**, 054314 (2016).
- [42] C. Drischler, A. Carbone, K. Hebeler, and A. Schwenk, *Phys. Rev. C* **94**, 054307 (2016).
- [43] J. W. Holt and N. Kaiser, *Phys. Rev. C* **95**, 034326 (2017).
- [44] C. Drischler, K. Hebeler, and A. Schwenk, [arXiv:1710.08220](https://arxiv.org/abs/1710.08220).
- [45] J. Simonis, K. Hebeler, J. D. Holt, J. Menéndez, and A. Schwenk, *Phys. Rev. C* **93**, 011302(R) (2016).
- [46] A. Tichai, J. Langhammer, S. Binder, and R. Roth, *Phys. Lett. B* **756**, 283 (2016).
- [47] B. R. Barrett, P. Navrátil, and J. P. Vary, *Prog. Part. Nucl. Phys.* **69**, 131 (2013).
- [48] A. Carbone, A. Polls, and A. Rios, *Phys. Rev. C* **88**, 044302 (2013).
- [49] V. Somà, A. Cipollone, C. Barbieri, P. Navrátil, and T. Duguet, *Phys. Rev. C* **89**, 061301(R) (2014).
- [50] S. K. Bogner, R. J. Furnstahl, and A. Schwenk, *Prog. Part. Nucl. Phys.* **65**, 94 (2010).
- [51] R. J. Furnstahl and K. Hebeler, *Rep. Prog. Phys.* **76**, 126301 (2013).
- [52] G. E. Brown, A. D. Jackson, and T. T. S. Kuo, *Nucl. Phys. A* **133**, 481 (1969).
- [53] S. Binder, A. Calci, E. Epelbaum, R. J. Furnstahl, J. Golak, K. Hebeler, H. Kamada, H. Krebs, J. Langhammer, S. Liebig, P. Maris, U.-G. Meißner, D. Minossi, A. Nogga, H. Potter, R. Roth, R. Skibiński, K. Topolnicki, J. P. Vary, and H. Witała (LENPIC Collaboration), *Phys. Rev. C* **93**, 044002 (2016).
- [54] R. Machleidt, “private communication,” (2017).
- [55] R. Machleidt, F. Sammarruca, and Y. Song, *Phys. Rev. C* **53**, R1483 (1996).